Proceedings World Geothermal Congress 2023
Beijing, China, April 17 – 21, 2023

Dynamic Bottom Hole Stress Reconstructing process induced by intensifier jet slotting in deep geothermal drilling

Huajian Wang[a]; Hualin Liao[a*]; Hedi Sellami[b]; John-Paul Latham[c]; Jiansheng Xiang[c]; Laurent Gerbaud[b]

a. School of Petroleum Engineering at China University of Petroleum (East China), Qingdao, 266580, China.

b. MINES ParisTech, PSL-Research University, Geosciences Research Center, Pau,64000 Pau, France.

c. Earth Science and Engineering, Imperial College London, London, SW7 2AZ, United Kingdom.

E-mail address：liaohualin2003@126.com (Hualin Liao)

Keywords: Deep Geothermal Drilling, Jet Slotting, Stress Release, Down Hole Pressures, Fluid-Solid Coupling

ABSTRACT

The deep geothermal reservoir is mainly hot dry rock with high yield strength, strong abrasiveness, high in-situ stress and poor drillability, which lowing the rate of penetration in deep geothermal drilling. Increasing hard rock drilling rates of deep geothermal reservoirs, a novel drilling technology to release stress of bottom hole rock by jet slotting is proposed, which based on ORCHYD project. At present, it is generally believed that high pressure water jet plays an auxiliary role in rock breaking and rock cleaning, the effect of stress release on bottom hole which has received only scant attention. In order to analyze the stress release effect by jet slotting, the jet features, the slotting characteristics with different jet pressure and the stress release process induced by jet slotting need to be studied. Firstly, the jet features with different outlet pressures are obtained by means of computational fluid dynamics. Secondly, based on the above jet features, the characteristics of slotting with different jet features are analyzed. Finally, the release process of effective stress in the slotting process is studied. The results show that the inlet pressure does not affect the length of potential core, which is about 6 times the nozzle diameter. Within the length of potential core, the impinging pressure is equal to the nozzle drop. The depth of the groove is mainly affected by the action time and jet pressure. When the pressure is 150MPa, the groove depth can reach to 15mm, and with the increasing diameter of the nozzle, the width of the groove keeps getting bigger and bigger. The expansion of the slotting range significantly increases the release efficiency of axial effective stress and enlarges the stress release range of axial effective stress, and the effective stress fluctuation of rock is obvious in the process of slotting. The axial effective stress release efficiency is hardly affected by the range of groove in the area the drilling bit acting and shows a slight increase with the expansion of the slotting range. The stress release method and results of simulations in this paper have a guiding signification for understanding the technique still further.

1. INTRODUCTION

To meet an increasing worldwide energy demand, access to geothermal energy from deep reservoirs will play a key role in the global energy supply [1-4]. One of the factors affecting the performance of deep drilling operations is linked to the difficulty of breaking deep rock formations with an acceptable rate of penetration (ROP), hence the geothermal reservoir mining methods have received extensive attention [5-6]. Indeed, when the bottom hole rocs are subjected to strong geostatic stresses (due to the weight of the overlying rock masses and their tectonic deformation history over geological time) and hydrostatic pressures (due to the weight of the drilling mud column inside the well being drilled) [7-10], the deep hard rocks become even stronger and less brittle when drilled by conventional drill bits.

To increase the rate of penetration(ROP) of deep geothermal reservoirs, the main methods are to develop novel drill bits[11], supporting tools[12], and enhanced drilling parameters[13]. At present, it is generally believed that high-pressure water jet plays an auxiliary role in rock breaking and rock cleaning, the effect of stress release on the bottom hole which has received only scant attention. Through the research, it is found that the ultra-high-pressure water jet in the bottom hole rotation process, since the high-pressure nozzles are arranged on the bit with a certain eccentricity, the high-pressure nozzles rotate around the axis of the bit during rotary drilling, thus realizing continuous rock destruction. Eventually, they cut circular grooves at the bottom of the well that cut off the rock at the bottom from the wall[14]. Increasing hard rock drilling rates of deep geothermal reservoirs, a novel drilling technology to release the stress of bottom hole rock by jet slotting is proposed, which is based on this phenomenon.

To verify the advancement of the proposed technology, the jet features, the slotting characteristics with different jet pressure and the stress release process induced by jet slotting need to be studied. Firstly, the jet features with different outlet pressures are obtained by means of computational fluid dynamics. Secondly, based on the above jet features, the characteristics of slotting with different jet features are analyzed. Finally, the release process of effective stress in the slotting process and the rock failure characteristic of slotted rocks are studied.

2. METHOD

In this part, we mainly introduce the numerical simulation methods and experimental methods involved in the article

2.1 Numerical model of jet impact on rock

2.1.1 Numerical method of jet features

The current numerical simulation methods of turbulence can be divided into direct numerical simulation method and indirect numerical simulation method. The direct numerical simulation method refers to the direct solution of the instantaneous turbulence governing equation. The non-direct numerical simulation method does not directly calculate the pulsation characteristics of

turbulence, but does some approximation and simplification of turbulence through certain means. Considering that the numerical model established in this paper is not very complicated and the existing computer conditions, the RNG k-ε turbulence model can meet the calculation accuracy requirements.

$$\begin{cases} \dfrac{\partial}{\partial t}(\rho k)+\dfrac{\partial}{\partial x_i}(\rho k u_i)=\dfrac{\partial}{\partial x_j}\left[\left(\mu+\dfrac{\mu_t}{\sigma_k}\right)\dfrac{\partial k}{\partial x_j}\right]+P_k-\rho\varepsilon \\ \dfrac{\partial}{\partial t}(\rho \varepsilon)+\dfrac{\partial}{\partial x_i}(\rho \varepsilon u_i)=\dfrac{\partial}{\partial x_j}\left[\left(\mu+\dfrac{\mu_t}{\sigma_\varepsilon}\right)\dfrac{\partial \varepsilon}{\partial x_j}\right]+C_{1\varepsilon}\dfrac{\varepsilon}{k}P_k-C_{2\varepsilon}^{*}\rho\dfrac{\varepsilon^2}{k} \end{cases} \tag{1}$$

$$C_{2\varepsilon}^{*}=C_{2\varepsilon}+\frac{C_\mu\eta^3(1-\eta/\eta_0)}{1+\beta\eta^3},\ \eta=\frac{Sk}{\varepsilon}=\frac{\left(2S_{ij}^2\right)^{1/2}k}{\varepsilon} \tag{2}$$

2.1.2 Physical model

For a constant pressurizing chamber pressure of 100 MPa,160 MPa, 205 MPa, 250 MPa, (achievable in lab and optimistic for field test), using exact Karcher 1 mm nozzle details as provided in attached drawings and described above: Note that the wall region(yellow/ green/black region in figure 1) defines a no inflow/outflow domain boundary, and the light blue region /red region at the left figure shows the fluid flow domain has a large outflow area given by the 14.5 mm wide annulus, and outflow boundary condition is with a zero pressure condition imposed. The center of the figure is the inlet with a diameter of 1mm. Impinging pressure distribution at boundary plate set at stand-off distance 3mm,6 mm and 10mm.

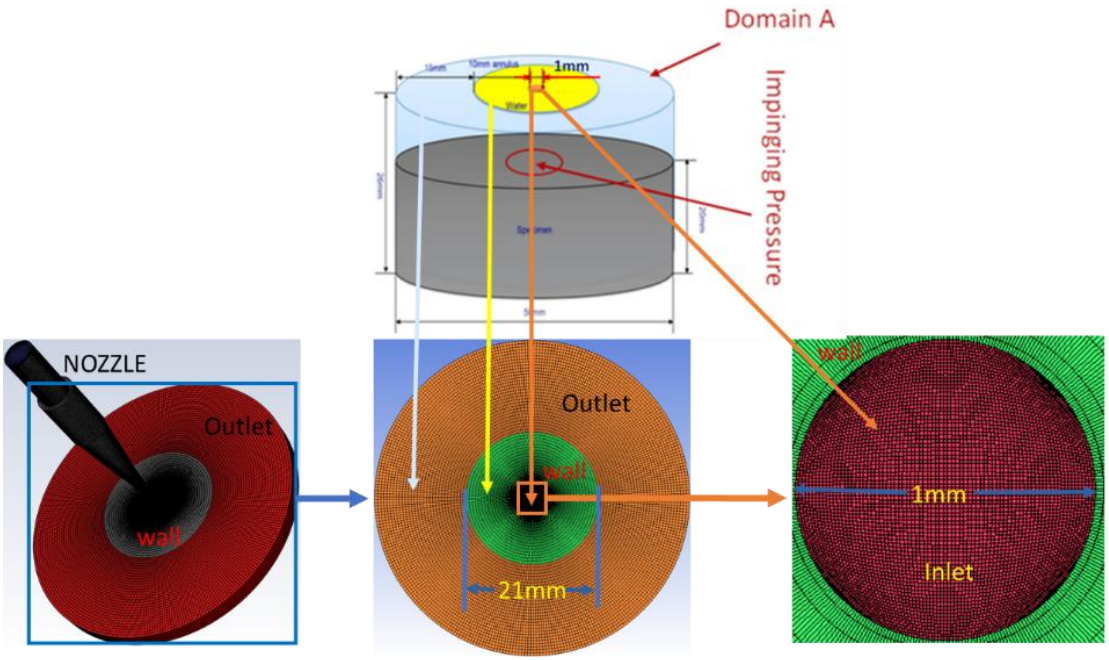

Fig.1 Schematic diagram of stagnation pressure model

2.2 Numerical method of bottom hole rock stress release

2.2.1 Numerical method of stress release

As overburden is converted to hydrostatic pressure by drilling, the rock matrix will be deformed. To describe the interaction between pore fluid and rock matrix, the rock is regarded as poroelasticity material[15]:

$$\sigma=C:\ \varepsilon-\alpha_B p_p I \tag{3}$$

where, σ is Cauchy stress tensor; ε is strain tensor; α_B is Biot-Willis coefficient; p_p is pore pressure; C is the elasticity matrix; I is the unit matrix; ":" stands for the double-dot tensor product.

$$\nabla\cdot-\frac{k_m}{\mu}\left(\nabla p_p-\rho_l g\right)+\left(\frac{\alpha-\varphi}{k_a}+\frac{\varphi}{k_l}\right)\frac{\partial p_p}{\partial t}+\alpha\frac{\partial \vartheta}{\partial t}=q_m \tag{4}$$

where, k_m is the permeability of the rock skeleton; μ is the fluid viscosity, ρ_l is the fluid density, $\frac{\alpha-\varphi}{k_a}$ is the compression term of rock skeleton; $\frac{\varphi}{k_l}$ is the compression term of fluid; k_a , k_l is the bulk modulus of the rock skeleton and fluid respectively; φ is the porosity; $\alpha\frac{\partial\vartheta}{\partial t}$ is the volumetric strain term; q_m is the source sink term[16].

2.2.2 Physical model

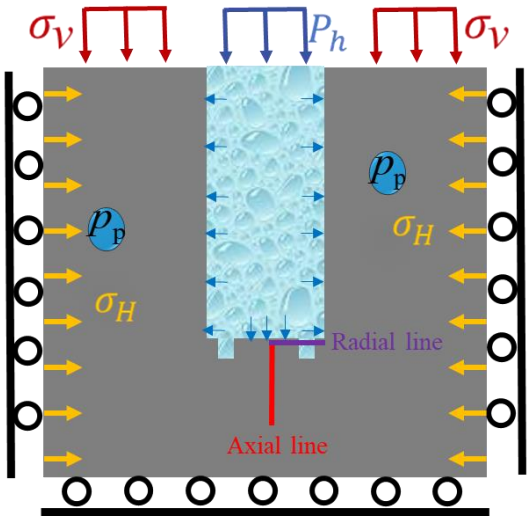

Figure 2 Petrophysical model of the rock at bottom-hole

The model of down-hole rock is established, in which the length of the model is 2400 mm, the width is 2400 mm and the height is 2000 mm, the wellbore diameter is 240 mm and its depth is 1200 mm. The simplified stress condition of deep rock is as shown in Fig. 2. The overburden is set at the top of the model, and the maximum horizontal crustal stress and minimum horizontal crustal stress are set at the surrounding of the model respectively. At the surrounding of the model and the bottom of the model is a set roller constraint. Hydrostatic pressure is set to the wellbore, and good permeability is assumed. The interaction between hydrostatic pressure and pore pressure is realized.

3 RESULTS AND DISCUSSION

3.1 Numerical simulation of jet features

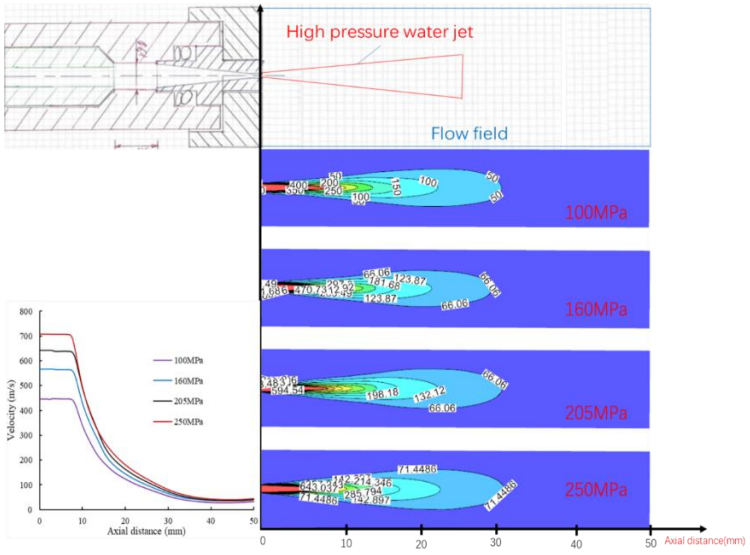

Figure 3 Velocity distribution along axial direction

As we can see from figure 7, With the increase of inlet pressure, the velocity of outlet increases, the velocity at 1 mm orifice outlet is 446m/s(100Mpa), 567 m/s(160Mpa), 643m/s(205Mpa) and 706 m/s(250Mpa) respectively, but the velocity at the far left nozzle

end (10mm) decays as 338 m/s (100Mpa), 443(160Mpa), 506 m/s(205Mpa) and 511 m/s(250Mpa) respectively, they are very different. Length of the potential core (7mm) is about 7 times the diameter of nozzle, in the potential core region (distance is 0mm to 7mm), the velocity is basically stable, and gradually decreases with the increasing of distance. in addition, the rate of decay is constantly decreasing with the increasing of distance.

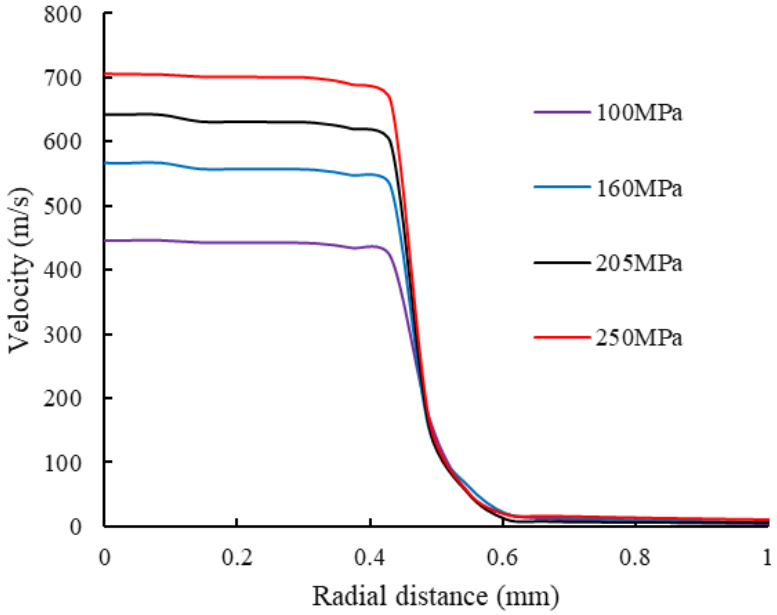

Fig.4 Velocity distribution along radial direction

Figure 4 shows the velocity distribution along radial direction at different pressures. As we can see from this picture, the maximum velocity is located at the axis, and the velocity decreases rapidly with the increase of radial distance, within the distance of 5mm, the velocity distribution along the radial direction is similar, and with the increase of the radial distance, the velocity decreases sharply. When the axial distance is more than 5 times the diameter of nozzle, with the increase of axial distance, the rate of velocity decay degree decreases gradually along radial director. The increase of inlet pressure increases the velocity but does not change the radial distribution of the velocity.

3.2 Numerical simulation and lab test of jet slotting

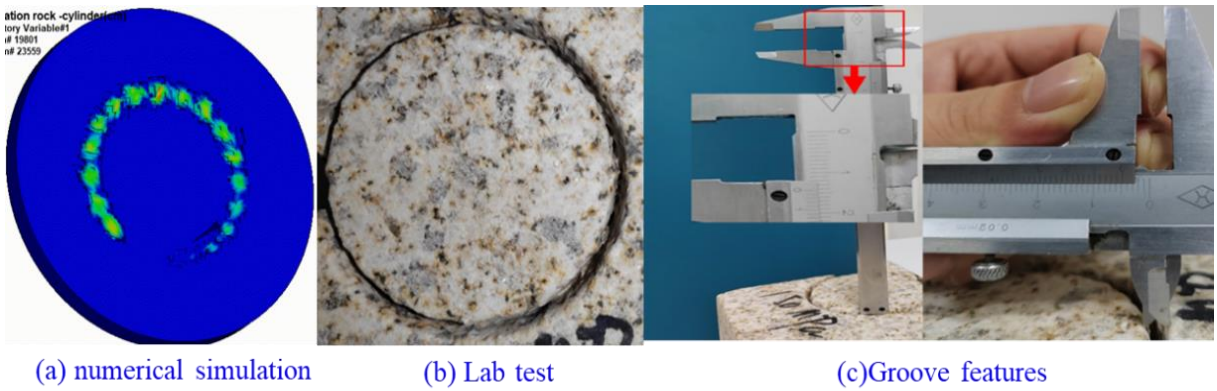

Figure 5 The characteristic of grooves induced by ultra high-pressure water jet

The characteristic of grooves induced by ultra high-pressure water jet has been studied (Figure 5). When the jet pressure is 150MPa, the groove depth can reach 15mm, and the higher the pressure of the water jet, the longer the acting time, the deeper the groove will be. It is also found that under certain conditions, water jet can generate a groove with a depth of 50mm.

In terms of width, under the condition of 0.5 mm nozzle diameter with a standoff distance of 10 times the nozzle diameter, the groove width can reach 5mm. Furthermore, in the drilling process, the nozzle with a diameter is 2mm will be used, and the groove is much wider.

3.3 Stress release characteristic of slotted rocks

Figure 6 and Figure 7 respectively show the distribution characteristics of radial effective stress and axial effective stress changing with radial position. By comparing Figure 6 and Figure 7, it is obvious that the distribution characteristics of the two are very similar, that is, the stress near the bottom hole center is very small. With the gradual increase of radial distance, both the radial effective stress and the axial effective stress show a gradual increase trend. The stress does not change when the hole radius is 0.9 times, and is stable

at the size of the initial in-situ stress. It is worth noting that the effective stress at the same position gradually decreases with the gradual increase of the groove Angle, which is caused by the gradual reduction of the compression degree of the horizontal in-situ stress on the rock at the bottom of the hole. The closer the wellbore axis is, the more obvious the effective stress decreases.

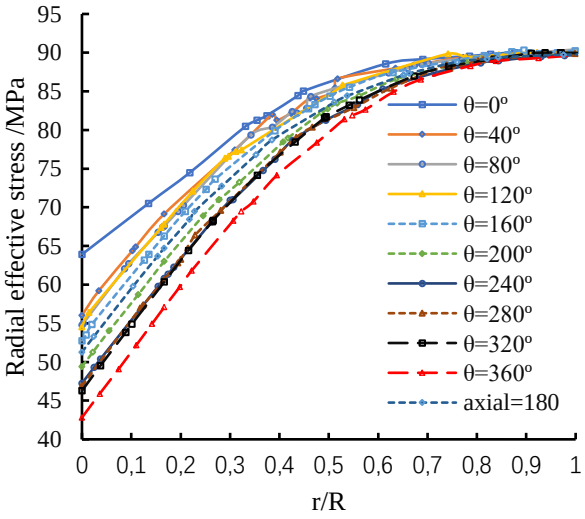

Figure 6 Radial effective stress along radial direction

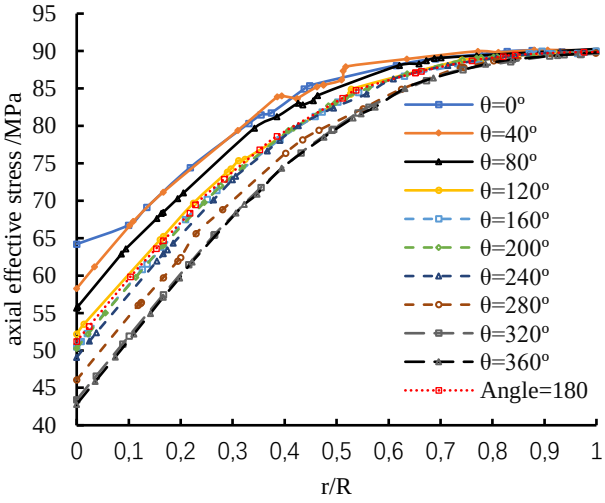

Figure 7 Axial effective stress along radial direction

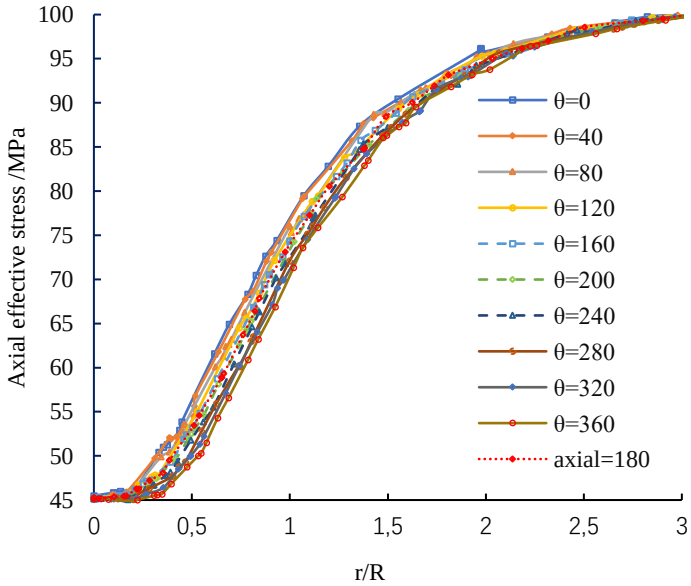

Figure 8 Axial effective stress along axial direction

Figure 8 shows the distribution characteristic of the axial effective stress along the axial position. The minimum axial effective stress at the center of the borehole is stable at about 45MPa, and the effective stress increases gradually with the gradual increase of the axial distance. And the axial effective stress also showed a decreasing trend with the gradual increase of the slotting range. However, compared with the distribution characteristics of the axial effective stress along the radial direction, the change of the axial effective stress along the axial position was not decreasing obviously.

3.4 The rock failure characteristic of slotted rocks

Figure 9 compares the distribution characteristics of cracks inside the rock and the distribution characteristics of cracks on the surface before and after grooving. After grooving, the number of cracks inside the rock increases obviously and the failure area also shows an increasing trend. In the rock surface area, the cracks around the crushing pit are mainly Hertzian cracks when the rock is not slotted. After the slotting, the cracks around the crushing pit gradually expand to the groove direction and finally connect with the groove. Therefore, under the same input conditions, the existence of grooves will significantly improve the rock crushing efficiency.

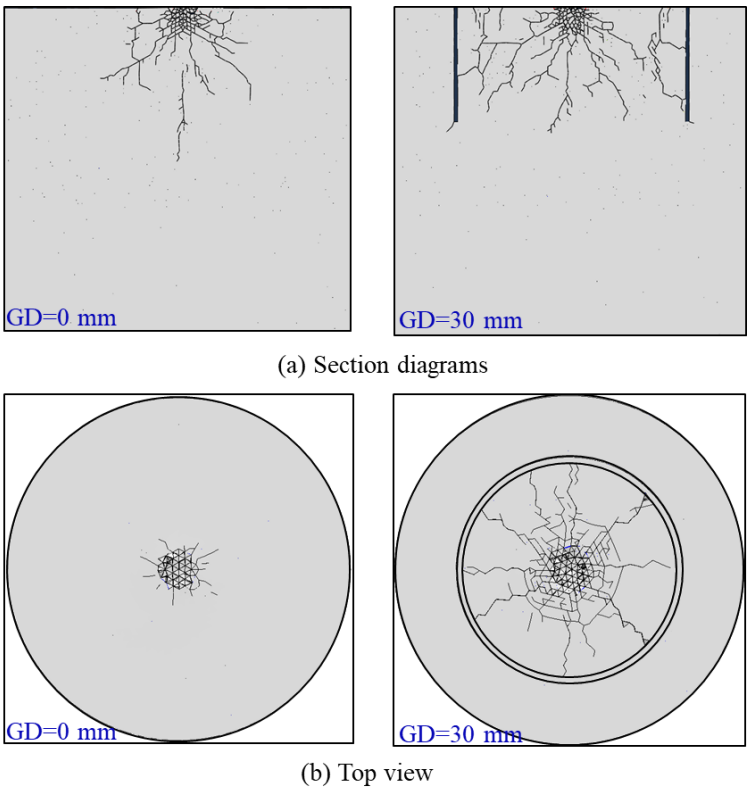

Figure 9 Axial effective stress along axial direction

Figure 10 shows the variation characteristics of peak impact force under different groove depths. The peak impact force gradually decreases with the increase of groove depth, but the peak impact force does not change when the groove depth reaches 20mm. By comparing the change of peak impact force when the groove is cut 20mm, the peak impact force is about 47% lower than that when the groove is not slot. This is because the stiffness of the slotted rock gradually decreases under the same impact energy condition, which not only protects the bit, but also facilitates continued rock breaking with the remaining energy in the bit.

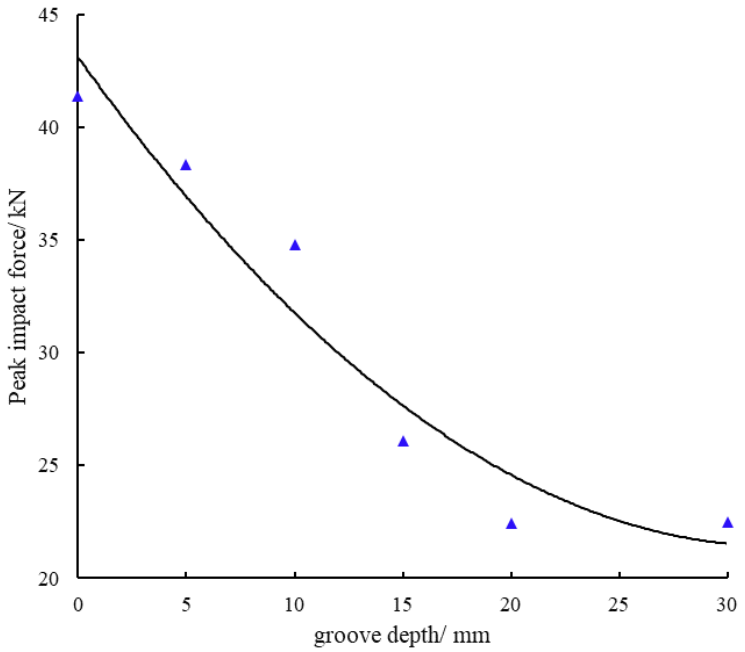

Figure 10 Axial effective stress along axial direction

CONCLUSIONS

The inlet pressure does not affect the length of potential core, which is about 7 times the nozzle diameter. Within the length of potential core, the impinging pressure is equal to the nozzle drop.In the potential core region (distance is 0mm to 7mm), the velocity

is basically stable, and gradually decreases with the increasing of distance. in addition, the rate of decay is constantly decreasing with the increasing of distance.

The depth of the groove is mainly affected by the action time and jet pressure. When the pressure is 150MPa, the groove depth can reach to 15mm, In terms of width, under the condition of 0.5 mm nozzle diameter with a standoff distance of 10 times the nozzle diameter, the groove width can reach 5mm.With the increasing diameter of the nozzle, the width of the groove keeps getting bigger and bigger. When the strength of the rock is low, the water jet can generate a groove with a depth of 50mm

The expansion of the slotting range significantly increases the release efficiency of axial effective stress and enlarges the stress release range of axial effective stress, and the effective stress fluctuation of rock is obvious in the process of slotting. The axial effective stress release efficiency is hardly affected by the range of groove in the area the drilling bit acting and shows a slight increase with the expansion of the slotting range.

After grooving, the number of cracks inside the rock increases obviously and the failure area also shows an increasing trend. In the rock surface area, the cracks around the crushing pit are mainly Hertzian cracks when the rock is not slotted. After the slotting, the cracks around the crushing pit gradually expand to the groove direction and finally connect with the groove. The peak impact force gradually decreases with the increase of groove depth, but the peak impact force does not change when the groove depth reaches 20mm. The advances and effectiveness of the novel drilling technology combining hydro-jet and percussion methods was verified.

REFERENCES

[1] Edoardo R, Shahin J, Volker W, Martin O, Saar, Philipp R. A combined thermo-mechanical drilling technology for deep geothermal and hard rock reservoirs. Geothermics2020;85:101771.

[2] Christopher F. Alternative energy sources. Applied Energy1994;47:123-146.

[3] Moore J, Simmons S. More power from below. Science 2013;340(6135):933–934.

[4] Chong Z, Yang S, Babu P, Linga P, Li X. Review of natural gas hydrates as an energy resource: Prospects and challenges. Appl Energy2016;162:1633–1652.

[5] Pan S, Gao M, Shah K, Zheng J, Pei S, Chiang P. Establishment of enhanced geothermal energy utilization plans: Barriers and strategies. Renew. Energ2019;132:19–32.

[6] Ma W, Wang Y, Wu X, Liu G. Hot dry rock (HDR) hydraulic fracturing propagation and impact factors assessment via sensitivity indicator. Renew. Energ2020;146:2716–2723.

[7] Chen P, Miska S, Yu M, Evren O. Poroelastic modeling of cutting bottom-hole rock – part i: stress state of bottom-hole rock - sciencedirect. J. Petrol. Sci. Eng2020;189:107014.

[8] Hu H, Guan Z, Xu Y, Han C, Liu Y, Liang D, Lu B. Bottom-hole stress analysis of ultra-deep wells based on theory of poroelastic mechanics. Journal of china university of petroleum (Edition of natural science)2020;44(5):52-61.

[9] Liao H,Wang H,Niu J,Wei J, Niu W, Liu J. Characteristics of stress release during downhole slotting by high-pressure water jet. Acta Petrolei Sinica2022;43(9):1325-1333.

[10] Wang H, Liao H, Wei J, Liu J, Niu W, Liu Y, Guan Z, Sellami, H, Latham J, Stress release mechanism of deep bottom hole rock by ultra-high-pressure water jet slotting, Petroleum Science 2023

[11] Xue Z. High speed high pressure impact resistant roller bit, CN201679448U. 2010.

[12] Zhao Y, Shi Z, Hu Z, Liu Q. Research and application of PDM borehole technology for HDD. Procedia earth and planetary science2011;3:183-188.

[13] Liao H, Guan Z, Shi Y, Liu Y. Field tests and applicability of downhole pressurized jet assisted drilling techniques. International journal of rock mechanics and mining sciences2015;75:140-146.

[14] Wang H, Liao H, Wei J. Liu Y, Niu W, Latham J, Xiang J, Liu J, Chen J. Pressure drop model and jet features of ultra high pressure water jet for downhole intensifier. ASME.J Energy ResourTechnol2022;144(12): 123005.

[15] Biot MA., 1962. Mechanics of deformation and acoustic propagation in porous media.J. Appl. Phys. 33: 1482–1498.

[16] Cheng LS., 2011. Advanced seepage mechanics[M], Beijing: Petroleum Industry Press.